Applications and Applied Mathematics: An International Journal (AAM)

Volume 16 | Issue 2 Article 16

12-2021

(R1480) Heat Transfer in Peristaltic Motion of Rabinowitsch Fluid in a Channel with Permeable Wall

Mahadev M. Channakote
Ramaiah University of Applied Sciences

Dilipkumar V. Kalse
Guru Nanak Dev Engineering College

Available at
http://pvamu.edu/aam
Appl. Appl. Math.
ISSN: 1932-9466

Applications and Applied Mathematics:
An International Journal
(AAM)

Vol. 16, Issue 2 (December 2021), pp. 1057 –1076

Heat Transfer in Peristaltic Motion of Rabinowitsch Fluid in a Channel with Permeable wall

[1*]Mahadev M. Channakote and [2]Dilipkumar V. Kalse
[1]Department of Mathematics and Statistics
M. S. Ramaiah University of Applied Science, Bengaluru
Karnataka 560058, India
email: mchannakote@rediffmail.com

[2]Department of Applied Sciences and Humanities
Gurunanak Dev Engineering College, Bidar
Karanataka 585403, India
email: kalsedilip@gmail.com
[*]Corresponding author

Received February 2, 2021; Accepted: September 9, 2021

Abstract

This paper is intended to investigate the effect of heat transfer on the peristaltic flow of Rabinowitsch fluid in a channel with permeable wall. The Navier-Stokes equations that governs the channel flow are constituted with Rabinowitsch fluid model. Corresponding equations are solved by utilizing approximations of the long-wavelength and small Reynolds number. The expressions for axial velocity, temperature distribution, pressure gradient, friction force, stream function is obtained. The influence of different physical parameters on velocity, pressure gradient, friction force, temperature and pumping action is explored via graphs.

Keywords: Peristaltic motion; Rabinowitsch fluid model; permeable wall; heat transfer; pressure; friction force

MSC 2010 No.: 76Z05, 76A05, 35C05

1. Introduction

Recently biologists, researchers, and scientists show deep interest in studying the problems of peristaltic flow of non-Newtonian fluid in tube/channel because of its increasing importance and extensive range of applications in a physiological, environmental, geophysical, and industrial process. In physiology, peristalsis plays a vital role in various situations such as urine transport from the kidney to bladder through the ureter, blood circulation in the small blood vessels, the transport of spermatozoa in the duct's afferents of the male reproductive tract, swallowing food through the esophagus, movement of chime in the gastro-intestinal tract, sanitary and corrosive fluids transport, and etc.

It is understood that in a physical and physiological phase, the filtration and mass transfer occur as fluid flows through a permeable tube. It is attributable to a great deal of application in real life, such as desalination by reverse osmosis, lymphatic drainage, and nephron tubules inflow. The pressure and velocity in these situations vary from the ordinary flow of Poiseuille in an impermeable tube since the fluid in contact with the wall may penetrate through the pores of the wall.

Due to its diverse applications in petroleum reservoir rocks, slurries, sedimentation, and sand beds the flow through porous medium received considerable attention by researchers and scientists. Examples of a porous medium in the human body include small blood vessels, human lungs, stone gallbladder, bile ducts, etc. Applying generalized Darcy's law peristaltic flow through a porous medium has been investigated by several researchers. Shehawey et al. (2000) studied the peristaltic motion of a generalized Newtonian fluid through a porous medium. The peristaltic pumping of a fluid with a varying viscosity in a non-uniform tube with a permeable wall has been reviewed by Vijay raj et al. (2005). Vajravelu et al. (2007) investigated the heat transfer on peristaltic flow of Newtonian fluid in a vertical porous annulus. A study of ureteral peristalsis in cylindrical tube through a porous medium is discussed by Rathod et al. (2011). Bhatti et al. (2016) investigated the effect of slip and magnetic field on Jeffrey fluid peristaltic flow in a porous medium. Sankad et al. (2016) examined the influence of permeable lining wall on the peristaltic flow of Herschel Bulkley fluid in a non-uniform inclined channel. The peristaltic flow of pseudoplastic fluid bounded by permeable walls with suction and injection was studied by Suresh Goud et al. (2017). Lakshminarayana et al. (2018) investigated the slip effect on a peristaltic flow of Bingham fluid in an inclined porous tube with joule heating. Rathod et al. (2011) studied the effect of thickness of the porous material on the peristaltic pumping of Jeffrey fluid with a non-erodible porous lining wall.

Numerous researchers studied the peristaltic flow through porous media with heat transfer due to its broad biophysical application. Vajravelu et al. (2007) studied peristaltic flow and heat transfer in a vertical porous annulus under long-wavelength approximation. Srinivas et al. (2009) investigated the influence of heat and mass transfer on MHD peristaltic flow through a porous space with a complaint wall. The influence of heat transfer on the peristaltic transport of a Jeffrey fluid in a vertical porous stratum has been investigated by Vajravelu et al. (2011). Vasudeva et al. (2011) addressed the effect of heat transfer on peristaltic flow of Jeffery fluid through a porous medium in a vertical channel. The influence of induced magnetic field and heat flux with the suspension of carbon nanotubes for the peristaltic flow in a permeable channel is reported by Noreen Sher Akbar et al. (2015). Tripathi (2013) examined the transient peristaltic heat flow through a finite porous medium. Rathod et al. (2014) investigated the interaction of heat transfer and peristaltic pumping of fractional second-grade fluid through a vertical cylindrical tube. Vajarvelu et al. (2016) analyzed heat transfer due to the nonlinear peristaltic transport of a Jeffrey fluid through a finite vertical porous channel.

Saleem et al. (2020) utilized a hybrid nanofluid to depict the peristaltic component within a curved tube with a ciliated wall. Sadaf and Nadeem (2020) examined the fluid flow and heat transfer of cilia beating in a curved channel in the presence of a magnetic field. Saleem et al. (2021) presented a computational research on the flow of heated non-Newtonian fluid within a sinusoidal elliptic duct. Saleem et al. (2021) investigated the peristaltic flow of Bingham viscoplastic micropolar fluid inside a microchannel with electro-osmotic effects. Saleem et al.

(2021) reported the physiological flow of a non-Newtonian fluid with variable density via a ciliated symmetric channel with a compliant wall

Rabinowitsch fluid is a class of pseudo-plastic fluids attracted much by the investigators; the application of this fluid model in peristalsis is very useful in physiology and biomedicine. Recently, Singh et al. (2013, 2014) have exhaustively studied about this fluid. Thanesh Kumar et al. (2017) investigated the influence of slip effects on the peristaltic flow of Rabinowitsch fluid in a non-uniform tube.

The Rabinowitsch fluid model was used to study the peristaltic flow in a channel with heat transfer by Singh et al. (2018). Akbar et al. (2014) discussed the Rabinowitsch fluid applications in peristaltic motion. Maraj et al. (2015) considered a curved channel to study the peristaltic flow of Rabinowitsch fluid. Existing literature indicates that little effort is made to study the peristaltic flow of Rabinowitsch fluid in a channel/tube.

Motivated by these studies, the heat transfer in the peristaltic motion of Rabinowitsch fluid in a channel with a permeable wall is investigated in this paper. The velocity, pressure rise, frictional force, temperature distribution, the stream function, and the volume flow rate are obtained. Some deductions are made, and results are found to agree with the earlier works.

Highlights and Novelty of the study

- The flow characteristics, trapping phenomenon, and heat generation of peristaltic flow of non-Newtonian fluid in a channel/tube with a permeable wall are analyzed. The Rabinowitsch model is incorporated in the study, and this model gives the flow characteristic of peristaltic transport in the channel/tube.
- The current study gives the bio fluid rheology of the complex flow through a tube with a muscular wall qualitatively. The study also predicts physiological flow characteristics (in particular blood) through a tube/channel with a permeable (muscular) wall.
- Further, this investigation provides qualitative information to regulate the flow and the temperature of the body by taking variables as control parameters with a suitable range.

2. Mathematical formulation

The peristaltic flow of Rabinowitsch fluid that is incompressible under the influence of permeable walls is considered. The flow is created by sinusoidal wave trains, which propagate along the channel walls with constant speed. Using a fixed frame as rectangular coordinates, Figure 1 presents a schematic diagram of the problem.

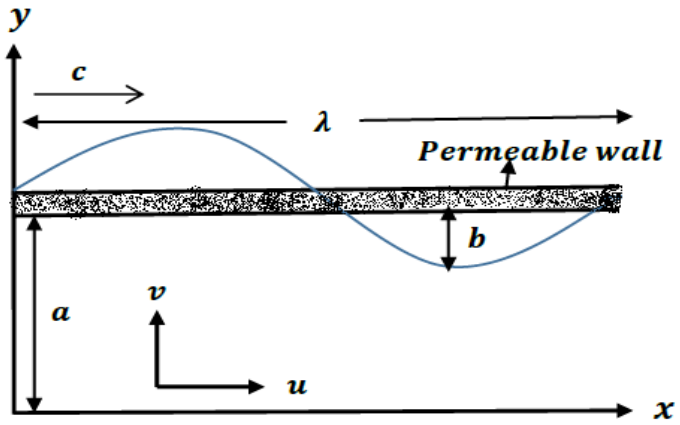

Figure 1. Flow geometry

The geometry of the wall surfaces is defined as

$$\mathrm{H}(\mathrm{X},\mathrm{t}') = a + \mathrm{b}\sin\left(\frac{2\pi(\mathrm{X}-\mathrm{ct}')}{\lambda}\right), \tag{1}$$

where λ is the wavelength, t' is time, a is the half of the channel width, b is the wave amplitude.

A well-established approach to analyze the non-Newtonian character of the fluid is the Rabinowitsch fluid model. For the Rabinowitsch fluid model, the shearing stress and shearing strain are related by the relationship as given below

$$S_{YX} + \gamma\, {S^3}_{XY} = \left(\mu\frac{\partial U}{\partial Y}\right), \tag{2}$$

where γ is the dimensional form of the parameter of the pseudo plasticity. The equations governing the flow in fixed frame of reference are given by:

$$\frac{\partial U}{\partial X} + \frac{\partial V}{\partial Y} = 0\,, \tag{3}$$

$$\rho\left(\frac{\partial U}{\partial t'} + U\frac{\partial U}{\partial X} + V\frac{\partial U}{\partial Y}\right) = -\frac{\partial p}{\partial X} + \frac{\partial S_{XX}}{\partial X} + \frac{\partial S_{YX}}{\partial Y}, \tag{4}$$

$$\rho\left(\frac{\partial V}{\partial t'} + U\frac{\partial V}{\partial X} + V\frac{\partial V}{\partial Y}\right) = -\frac{\partial p}{\partial Y} + \frac{\partial S_{YX}}{\partial X} + \frac{\partial S_{YY}}{\partial Y}, \tag{5}$$

$$\rho c_p\left(\frac{\partial T}{\partial t'} + U\frac{\partial T}{\partial X} + V\frac{\partial T}{\partial Y}\right) = K\left(\frac{\partial^2 T}{\partial X^2} + \frac{\partial^2 T}{\partial Y^2}\right) + S_{XX}\frac{\partial U}{\partial X} + S_{YY}\frac{\partial V}{\partial Y} + S_{YX}\left(\frac{\partial U}{\partial Y} + \frac{\partial V}{\partial X}\right). \tag{6}$$

In the above equations, U and V are components of velocity in (X , Y) directions respectively in fixed reference frames, ρ is density, p is pressure, T is temperature, K is thermal conductivity, c_p is specific heat at constant pressure, t' is time, S_{XX}, S_{YX}, S_{YY} are stress tensor components.

The transformation between wave and the fixed frame is defined by:

$$u' = U - c, v' = V, \tag{7}$$

$$x' = X - ct', y' = Y, \tag{8}$$

where u', x', v', y' axial velocity, axial coordinate, transverse velocity, and transverse coordinates are respectively in wave frame.

The transformations used in the above equations are in scale:

$$u = \frac{u'}{c}, v = \frac{v'}{c\delta}, x = \frac{x'}{\lambda}, y = \frac{y'}{a}, h = \frac{H}{a}, \delta = \frac{a}{\lambda}, p = \frac{p' a^2}{\mu\, c\, \lambda}, Re = \frac{\rho\, c\, a}{\mu}, \theta = \frac{T - T_0}{T_0},$$

$$t = \frac{ct'}{\lambda}, Pr = \frac{\mu\, c_p}{K}, Ec = \frac{c^2}{c_p T_0}, \phi = \frac{b}{a}, S_{xy} = \frac{a\, S'_{xy}}{c\mu}, S_{xx} = \frac{a\, S'_{xx}}{c\mu}, \alpha = \frac{c^2 \mu^2}{a}\gamma, \tag{9}$$

where δ is the wavenumber, Pr is the Prandtl number, Ec is the Eckert number, ϕ is the amplitude ratio, and α is the pseudo-plasticity parameter, respectively.

Using the above non-dimensional quantities of equations (7) - (9) and taking long wavelength ($\delta \ll 1$) and low Reynolds number approximations ($Re \approx 0$), equations (1) - (6) reduces to:

$$S_{yx} + \alpha\, S^3{}_{yx} = \frac{\partial u}{\partial y}, \tag{10}$$

$$h = 1 + \phi \sin(2\pi x), \tag{11}$$

$$\frac{\partial p}{\partial x} = \frac{\partial S_{yx}}{\partial y}, \tag{12}$$

$$\frac{\partial p}{\partial y} = 0, \tag{13}$$

$$\frac{\partial^2 \theta}{\partial y^2} = -Br\, S_{yx} \frac{\partial u}{\partial y}, \tag{14}$$

where $Br = EcPr$ is the Brinkman number.

The boundary conditions corresponding to Saffaman are given by:

$$\frac{\partial u}{\partial y} = 0 \text{ at } y = 0, \;\; u = -1 - \frac{\sqrt{Da}}{\eta}\frac{\partial u}{\partial y} \;\; \text{at } y = h, \tag{15}$$

$$\frac{\partial \theta}{\partial y} = 0 \text{ at } y = 0, \;\; \theta = 0 \;\; \text{at } y = h, \tag{16}$$

where, Da is Darcy number and η is the slip parameter.

3. Solution of the problem

Solving equation (12) using the boundary condition (15), we get

$$u = \left(\frac{y^2-h^2}{2}\right)\frac{dp}{dx} + \alpha\left(\frac{dp}{dx}\right)^3\left(\frac{y^4-h^4}{4}\right) - \frac{\sqrt{Da}}{\eta}\left(h\frac{dp}{dx} + h^3\left(\frac{dp}{dx}\right)^3\alpha\right) - 1\,. \tag{17}$$

Again, solving equation (14) using the boundary condition (16), we obtain

$$\theta = Br\left(\frac{dp}{dx}\right)^2\left(\frac{(h^4-y^4)}{12} + \alpha\,\frac{(h^6-y^6)}{30}\left(\frac{dp}{dx}\right)^2\right). \tag{18}$$

In terms of the stream function relationship, velocities can be defined as $u = \frac{\partial\psi}{\partial y}, v = -\frac{\partial\psi}{\partial x}$.

Integrating equation (17) and using the condition $\psi = 0$ at $y = 0$ we get

$$\psi = \left(\frac{y^3}{6} - \frac{y\,h^2}{2}\right)\frac{dp}{dx} + \alpha\left(\frac{dp}{dx}\right)^3\left(\frac{y^5}{20} - \frac{y\,h^4}{4}\right) - \sqrt{Da}\,h\,y\frac{\frac{dp}{dx}\left(1+h^2\left(\frac{dp}{dx}\right)^2\alpha\right)}{\eta} - y\,. \tag{19}$$

The volume flow rate Q' in the fixed frame is given by:

$$Q' = \int_0^H U\,dy, \tag{20}$$

The volume flow rate q' in wave frame is defined as:

$$q' = \int_0^h u\,dy. \tag{21}$$

Using equation (7), one can finds that the two volume flow rates are related by

$$Q' = q' + cH, \tag{22}$$

The time mean flow over a period $T = \frac{\lambda}{c}$ at a fixed position X is defined as

$$\tilde{Q} = \frac{1}{T}\int_0^T \bar{Q}\;dt, \tag{23}$$

which can be written, using equation (21) and (22)

$$\tilde{Q} = q' + ca\,, \tag{24}$$

Defining the dimensionless time-mean flow Q and q in the fixed and wave frame respectively as

$$Q = \frac{\tilde{Q}}{a\,c} \text{ and } q = \frac{q'}{a\,c}, \tag{25}$$

then making use of (25), equation (24) can be written as

$$Q = q + 1, \tag{26}$$

where

$$q = \int_0^h u\, dy, \tag{27}$$

Using equation (17) in equation (27), we get:

$$\frac{dp}{dx} + \frac{3}{5}\,\alpha\, h^2 \left(\frac{dp}{dx}\right)^3 + 3\left(\frac{q+h}{h^3}\right) + \frac{3\sqrt{Da}}{\eta\, h^3}\left(h^2\frac{dp}{dx} + h^4\left(\frac{dp}{dx}\right)^3 \alpha\right) = 0. \tag{28}$$

It is tedious to obtain the analytical solution of equation (28) due to nonlinearity. Thus, the solution is obtained by using regular perturbation method. In order to apply perturbation technique, we expand $\frac{dp}{dx}$ in terms of the pseudo-plasticity parameter($|\alpha| \ll 1$) as follows:

$$\frac{dp}{dx} = p_0 + \alpha\, p_1\,. \tag{29}$$

The solution of equation (28) is given by:

$$\frac{dp}{dx} = -3\left(\frac{q+h}{h^3 + \frac{3\,h^2\sqrt{Da}}{\eta}}\right) + \alpha\,\frac{81\,(q+h)^3\left(h+\frac{5\sqrt{Da}}{\eta}\right)}{5h^4\left(h+\frac{3\sqrt{Da}}{\eta}\right)^4}\,. \tag{30}$$

Using equation (26) in equation (30), we get:

$$\frac{dp}{dx} = -3\left(\frac{Q-1+h}{h^3 + \frac{3\,h^2\sqrt{Da}}{\eta}}\right) + \alpha\,\frac{81\,(Q-1+h)^3\left(h+\frac{5\sqrt{Da}}{\eta}\right)}{5h^4\left(h+\frac{3\sqrt{Da}}{\eta}\right)^4}\,. \tag{31}$$

The results presented above corresponds to the results of Singh et al. (2018) as $Da \to 0$.

The pressure rise and friction force are respectively given by:

$$\Delta p = \int_0^1 \frac{\partial p}{\partial x}\, dx\,, \tag{32}$$

$$F = \int_0^1 h\,\left(-\frac{dp}{dx}\right) dx. \tag{33}$$

4. Results and Discussion

In this section, we present a qualitative study of the results obtained in the previous sections by varying the parameters. Our parameters of interest are pseudo-plasticity α, amplitude ratio ϕ, Darcy number Da, and slip parameter η and flow rate Q for Rabinowitsch fluid. The nature of the fluid is Newtonian for the parameter of pseudo-plasticity $\alpha = 0$, dilatants (Shear thinning) for $\alpha < 0$, and pseudoplastic (shear thickening) for $\alpha > 0$.

Figures 2-5 are sketched to analyze the flow characteristics of a Newtonian and non-Newtonian fluid. Figure 2 shows variation of velocity profiles for various values of Q and α. In shear

thickening fluid it is observed that the flow rate favors the fluid motion by increasing the magnitude of the velocity while Q opposes the fluid motion in the case of shear thinning fluid. Here it is noted that for shear thickening fluid the magnitude of the velocity increases and decreases with an increase in flow rate for shearthinning fluid. The velocity magnitude for Newtonian fluid is noted to be maximum in the center of the channel this is due to the absence of the shear stress. The opposite conduct can be seen on the channel wall. A similar effect is observed in Figure 3 with an increase in the value of amplitude ratio on velocity profiles.

Figures 4 and 5 are drawn to study the effect of the Rabinowitsch fluid parameter in the case of shearthinning and shearthickening on velocity distribution u for different values of Darcy number and slip parameter. Figure 4 depicts that with an increase in the value of Darcy number the magnitude of velocity increases for shearthinning and shearthickening fluid while an opposite trend is observed for a Newtonian fluid. It is often shown that the opposite activity can be seen on the wall of the channel.

From Figure 5 it is seen that the magnitude of velocity in the center of the channel is found the highest for a Newtonian fluid. The magnitude of velocity reduces for pseudo-plastic fluid and improves fluid consistency with an enhanced slip parameter for dilatant fluid.

It is well known fact that the fluid flow with high velocity exerts a high-pressure gradient and the same results are restated in Figures 6 - 9 for Rabinowitsch fluid. Figures 6 and 7 represent pressure gradient behavior with a change in amplitude ratio and flow rate. Unrecognizable variability in the pressure gradient is observed for $x \in [0,0.5]$ when the value of ϕ changes. A comparative analysis shows that in the case of the shearthickening fluid the pressure gradient in the narrow channel component is greater than that of the shearthinning fluid. Moreover, it is seen that with the increase in ϕ the pressure gradient increases (see Figure 6). From Figure 7, it is clear that the pressure gradient starts decreasing when the flow rate Q increases. The pressure gradient is very small for $x \in [0,0.6]$, and a large pressure gradient occurs for $x \in [0.6,0.9]$.

Figure 8 shows the impact of Darcy number Da on the pressure gradient. It is seen that the pressure gradient decreases with an increase in Darcy number. The highest-pressure gradient is observed in the case of dilatant fluid and the lowest pressure gradient is found in the narrow part of the channel for pseudo plastic fluid. Figure 9 present the variation of $\frac{dp}{dx}$ over one wavelength for different values of slip parameter η. From Figure 9 we observe that the pressure gradient is relatively small in the wider part of the channel. It is examined that the pressure gradient increases with the rising values of η.

Numerical integration is carried out in order to evaluate pumping characteristics and the results of variation of the pressure rise Δp against the average time flow rate Q, are shown in Figures 10 - 13.

From Figure 10 one can notice that the pressure rise increases for Newtonian fluid when ϕ increases in the area of the peristaltic pumping region ($Q > 0, \Delta p > 0$) whereas pressure rise shows an opposite attitude in the co-pumping region ($Q > 0, \Delta p < 0$). The fluid will be lean

when the pseudo-plasticity parameter is more, and a little pressure rise is noticed in the pumping area as compared to Newtonian and dilatant fluids. The maximum pressure rise observed for shearthinning fluid at zero flow rate.

Figure 11 demonstrates the effect of amplitude ratio ϕ on pressure rise for the material parameters $\alpha = -0.1, 0, 0.1$ and $Q = 0.3, 0.4$. It is noted that, for a Newtonian and dilatant type of fluid, the pressure rise increases at a steady flow rate but for pseudo-plastic fluid, and the pressure rise increases first and then reduces afterward. The pressure rise decreases at zero amplitude ratio with no pumping region as the flow rate increases.

Figure 12 shows the variation of Δp with flow rate Q for various values of the parameter of pseudo-plasticity $\alpha = -0.1,0,0.1$ and $Da = 0.001,0.002$. We observe that the pressure rise decreases with an increase of Da in the pumping region($Q > 0, \Delta p > 0$) where as behavior is opposite in the augmented pumping region ($Q > 0, \Delta p < 0$). An increase in Darcy number increases the permeability of the porous medium. Thus, ease with which the fluid flow is increased caused decrease in the pressure rise.

The impact of slip parameter η on the pressure rise for material parameters α is presented in Figure 13. We observe that the pumping curves intersect at a point where $Q = 0.25$ (approximately) in the pumping region ($\Delta p > 0, Q > 0$). When Q is less than 0.25 the pumping rate increases by increasing slip parameter η. After a critical value of Q that is $Q = 0.3$, the pumping rate increases when η is increased. Moreover, it is seen that increasing η causes increase in pressure rise which is greater as compared to that of the Newtonian and dilatant case while its behavior is quite opposite in the augmented region ($Q > 0,\ \Delta p < 0$).

Figures 14 - 17 display the difference in frictional force against flow rate. These Figures show that for all the relevant parameters, the frictional force has quite opposite features compared to pressure rise.

The distribution of temperature is investigated and depicted through Figures 18-21. Figure 18 shows the variation of temperature profile with y for $Br = 0.4, 0.5, \alpha = -0.1, 0, 0.1, Q = 0.8$, $\phi = 0.4, Da = 0.0001, \eta = 0.1, x = 0.2$.The temperature profiles are found to increase with increasing Brinkman number values as seen in Figure 18. It is shown here that the temperature profile is an increasing feature for pseudoplastic, dilatant, and Newtonian fluids. There is a greater heat generation due to friction since higher values Br are used by shear in the flow that raises the temperature of the fluid.

Figure 19 illustrates that the temperature profile is decreasing with increasing values of amplitude ratio for pseudoplastic fluids while increasing with increasing values of amplitude ratio for Newtonian and dilatant fluids. High temperature is observed in the center of the channel and decrease near the wall of the channel for Newtonian, pseudo-plastic, and dilatant fluids.

Figures 20 and 21 are drawn to study the effect of Rabinowitsch fluid parameter α on temperature distribution θ for various values of Darcy number Da and the slip parameter η. Figure 20 reveals that high temperature is observed at the center of the channel for all three

types of fluids. It is also observed the temperature field decreases with an increase in Darcy number. In Figure 21 we found that an increase in slip parameter η results in the increase of temperature θ. It is found that in comparison with the Newtonian case, the magnitude of temperature for shear thickening fluid $(\alpha < 0)$ is more than the shearthinning fluid $(\alpha > 0)$.

The next most interesting aspect of peristaltic flow is trapping which is taken into account by drawing streamlines against various physical parameters. The inviscid fluid streamlines are very helpful to understand the relationship between velocity and pressure. Figure 22 demonstrates the effects of α on the size and circulation of the trapped bolus. It is found that when the nature of the fluid changes gradually from pseudo-plastic fluid to dilatant the size of the bolus decreases. It is also analyzed that the number of boluses is more for Newtonian fluid as compared to pseudo-plastic and dilatant fluids. Streamlines are plotted in Figures 23 and 24 to see the effect of Darcy number Da and slip parameter η. Evidently, the number and size of trapping bolus for Newtonian fluid is greater as compared to pseudo plastic and dilatant fluids. It can also be noted that the number of boluses decreases for increasing the Darcy number Da but the number of trapped bolus increases for increasing slip parameter η.

5. Conclusions

The peristaltic flow of Rabinowitsch fluid is considered in a channel, in the wave frame of reference moving with velocity of the wave. Long-wavelength and low Reynolds number approximation is applied to resolve the model. Solutions are obtained for velocity, pressure gradient, pressure difference Δp, frictional force, temperature θ, and stream function.
The main outcomes of present investigations are:

- It is specifically observed that the magnitude of velocity for Newtonian fluid in the center of the channel is maximal and decreases with shearthinning fluid but increases with shear thickening fluid.
- The pressure gradient decreases with an increase in Darcy number.
- The of velocity increases with dilatant fluid and, with an increase in flow rate, reduces the pseudo-plastic quality of the fluid.
- In shearthinning situations, the temperature profiles decrease and the opposite behavior is observed in dilatant and Newtonian fluids.
- Temperature spectrum decreasing with rising Darcy number for all fluid types.
- The temperature for all three fluids increases with increasing slip parameter values.
- Frictional forces can be seen as having the opposite behavior to that of increasing energy.
- As a consequence of the rising amplitude ratio, the size of the trapped bolus decreases.
- In the case of shearthinning and shearthickening aspect of the stream, the size and quantity of the bolus are decreasing with an increase in Darcy value

Acknowledgements

The authors are immensely grateful to the Editor and reviewers for their insight and constructive suggestions that have been enable us to improve the quality of the manuscript.

REFERENCES

Bhatti, M.M and Ali Abbas, M. (2016). Simultaneous effect of slip and MHD on peristaltic blood flow of Jeffrey fluid model through porous medium, Alexandria Engineering Journal, Vol.5 (2), pp.1017-1023.

El Shehawey, E.F., Sobh, A.M.F. and El Barbary, E.M.E. (2000). Peristaltic motion of a generalized Newtonian fluid through porous medium, Journal of the Physical Society of Japan, Vol.69, pp. 401-407.

Lakshminarayana, P., Vajravelu, K., Sucharitha, G. and Sreenadh, S. (2018). Peristaltic slip flow of a Bingham fluid in an inclined porous conduit with joule heating, Applied Mathematics and Nonlinear Science, Vol.3 (1), pp. 41-54.

Maraj, E.N., Nadeem, S. (2015). Application of Rabinowitsch fluid model for the mathematical analysis of peristaltic flow in a curved channel, Z. Naturforsch, Vol. 70, pp. 513-520.

Mekheimer, K.H.S. (2003). Nonlinear peristaltic transport through a porous medium in an inclined planar channel, Journal of Porous Media, Vol.6, pp. 190-202.

Noreen Sher Akbar, Raza, M. and Ellahi, R. (2015). Influence of induced magnetic field and heat flux with the suspension of carbon nanotubes for the peristaltic flow in a permeable channel, Journal of Magnetism and Magnetic Materials, Vol.381(1), pp. 405-4015.

Noreen Sher Akbar and Nadeem, S (2014). Application of Rabinowitsh fluid Model in peristalsis, Z. Naturforsch, Vol.69a, pp. 473-480.

Ramachandra, R.A. and Mishara, M (2004). Peristaltic transport of a power law fluid in a porous tube, Journal of Non-Newtonian Fluid Mechanics, Vol.121, pp. 163-174.

Rathod V.P. and Channakote, M.M. (2011). A study of ureteral peristalsis in cylindrical tube through porous medium, Advances in Applied Science Research, Vol.3 (2), pp. 134-140.

Rathod, V.P. and Mahadev, M. (2011). Effect of thickness of the porous material on the peristaltic pumping of Jeffrey fluid with non-erodible porous lining wall, International Journal of Mathematical Archive, Vol.2 (10), pp.1-10.

Rathod, V.P. and Mahadev, M. (2014). Interaction of heat transfer and peristaltic pumping of frictional second grade fluid through a vertical cylindrical tube, Thermal Science, Vol. 18(4), pp. 1109-1118.

Sankad, G.C. and Asha, Patti. (2016). Impact of permeable lining of the wall on the peristaltic flow of Herschel Bulkley fluid, Applications and Applied Mathematics, Vol. 11(2), pp. 663-679.

Singh, B.K. and Singh, U.P. (2014). Analysis of peristaltic flow in a tube: Rabinowitsch fluid model, International Journal of Fluid Engineering, Vol.1, pp. 1-8.

Singh, U.P. Amit Medhavi, Gupta, R.S. and Siddarth Shanker Bhatt. (2018). Theoretical study of heat transfer on peristaltic transport of non-Newtonian fluid flowing in a channel, Rabinowitsch fluid model, International Journal of Mathematical, Engineering and Management Sciences, Vol.3 (4), pp. 450-471.

Suresh Goud, J. and Hemadri Reddy, R. (2017). Peristaltic transport of a pseudoplastic fluid bounded by permeable walls with suction and injection, International Journal of Pure and Applied Mathematics, Vol.113 (6), pp. 289-297.

Saleem, A., Kiani, M. N., Nadeem, S., Akhtar, S., Ghalambaz, M., and Issakhov, A. (2021). Electroosmotically driven flow of micropolar Bingham viscoplastic fluid in a wavy microchannel, Application of computational biology stomach anatomy. Computer Methods in Biomechanics and Biomedical Engineering, Vol. 24(3), pp.289-298.

Saleem, A., Qaiser, A., Nadeem, S., Ghalambaz, M., and Issakhov, A. (2021). Physiological flow of non-Newtonian fluid with variable density inside a ciliated symmetric channel having compliant wall. Arabian Journal for Science and Engineering, Vol.46 (1), pp.801-812.

Saleem, A., Akhtar, S., Alharbi, F. M., Nadeem, S., Ghalambaz, M., and Issakhov, A. (2020). Physical aspects of peristaltic flow of hybrid nano fluid inside a curved tube having ciliated wall. Results in Physics, Vol.19, pp.103431.

Saleem, A., Akhtar, S., Nadeem, S., Alharbi, F. M., Ghalambaz, M., and Issakhov, A. (2020). Mathematical computations for peristaltic flow of heated non-Newtonian fluid inside a sinusoidal elliptic duct. Physica Scripta, Vol. 95(10), pp.105009.

Sadaf, H. and Nadeem, S. (2020). Fluid flow analysis of cilia beating in a curved channel in the presence of magnetic field and heat transfer. Canadian Journal of Physics, Vol. 98(2), pp.191-197.

Thanesh Kumar, K. and Kavitha, A. (2017). The influence of slip effect on peristaltic transport of a Rabinowitsch fluid model in a non-uniform tube, IOP Conference Series: Material science and engineering, Vol. 263, pp. 1-12.

Tripathi, D. (2013). Study of transient peristaltic heat flow through a finite porous channel, Mathematical and Computer Modelling, Vol. 57, pp. 1270–1283.

Vajravelu, K., Sreenadh, S., Lakshminarayana, P. and Sucharitha, G. (2016).The effect of heat transfer on the nonlinear peristaltic transport of a Jeffrey fluid through a finite vertical porous channel, International Journal of Bio Mathematics, Vol. 9(2),pp. 1-24.

Vajravelu, K., Sreenadh, S., and Lakshminarayana, P. (2011). The influence of heat transfer on peristaltic transport of a Jeffrey fluid in a vertical porous stratum, Communications in Nonlinear Science and Numerical Simulation, Vol. 16(8), pp. 3107–3125.

Vajravelu. K., Radharishnamacharya, G. and Radhakrishna-Murthy, V. (2007). Peristaltic flow and heat transfer in a vertical porous annulus, with long wave approximation, International Journal of Non-Linear Mechanics, Vol. 42, pp.754 – 759.

Vasudev, C., Rajeswara Rao, U., Subha Reddy, M.V. and Prabhakara Rao, G. (2011). Effects of heat transfer on the peristaltic flow of Jeffrey fluid through a porous medium in a vertical annulus, Journal of Basic and Applied Scientific Research, Vol. 1(7), pp. 751-758.

Vasudev, C., Rajeswara Rao, U. and Subha Reddy, M.V. and Prabhakara Rao, G. (2010). Effect of heat transfer on Peristaltic transport of a Newtonian fluid through a porous medium in an asymmetric vertical channel, European Journal of Scientific Research, Vol. 44(1), pp.79-92.

Vijayaraj, K., Krishnaiah, G. and Ravi Kumar, M.M. (2005). Peristaltic pumping of a fluid of variable viscosity in a non-uniform tube with permeable wall, Journal of Theoretical and Applied Information Technology, Vol. 8(1), pp. 82-91.

APPENDIX

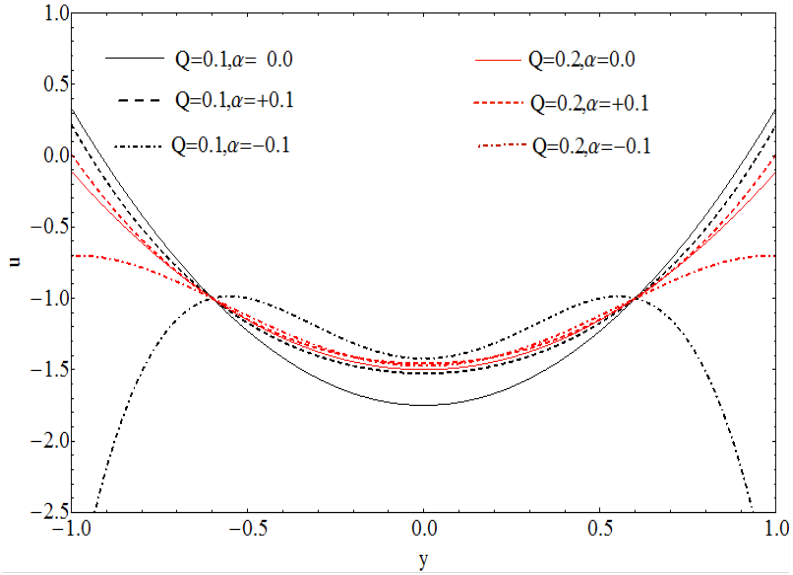

Figure 2. Velocity profile for various values of Q, α at $Da = 0, \eta = 1, \phi = 0.4, x = 0.75$

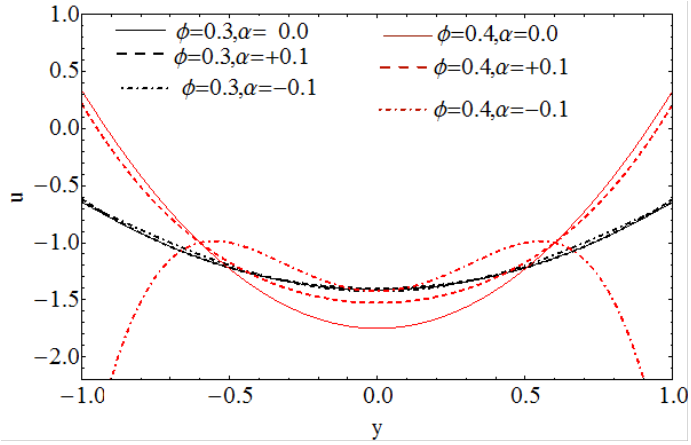

Figure 3. Velocity profile for various values of ϕ, α at $Da = 0.001, \eta = 1, Q = 0.1, x = 0.75$

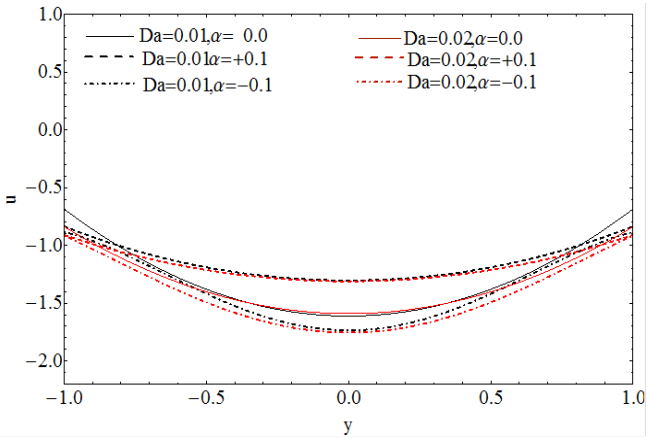

Figure 4. Velocity profile for various values of Da, α at $\phi = 0.4\,, \eta = 1, Q = 0.1, x = 0.75$

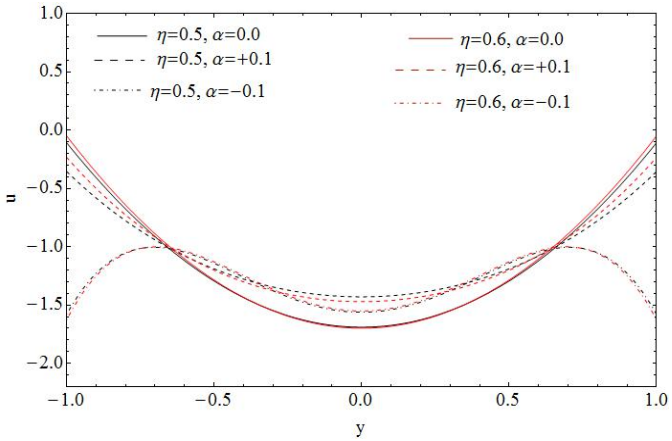

Figure 5. Velocity profile for various values of η, at $\phi = 0.4\,, Da = 0.001, Q = 0.1, x = 0.75$

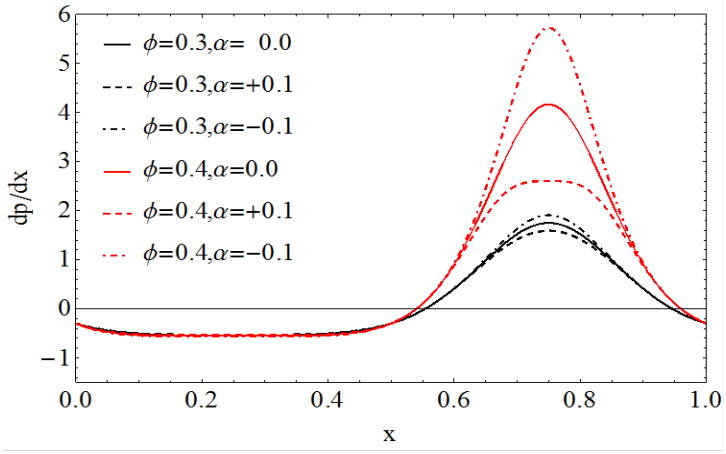

Figure 6. Pressure gradient for different values of ϕ, α. at $Q = 0.1,\ Da = 0, \eta = 1$

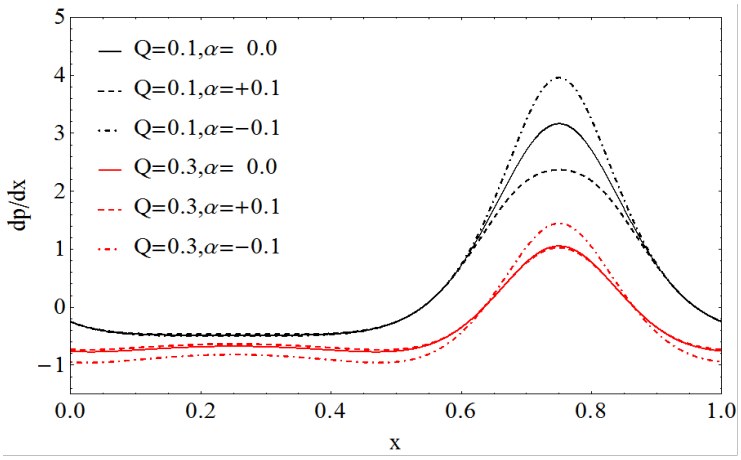

Figure 7. Pressure gradient for different values of Q, α.at $\phi = 0.3,\ Da = 0.001, \eta = 0.5$

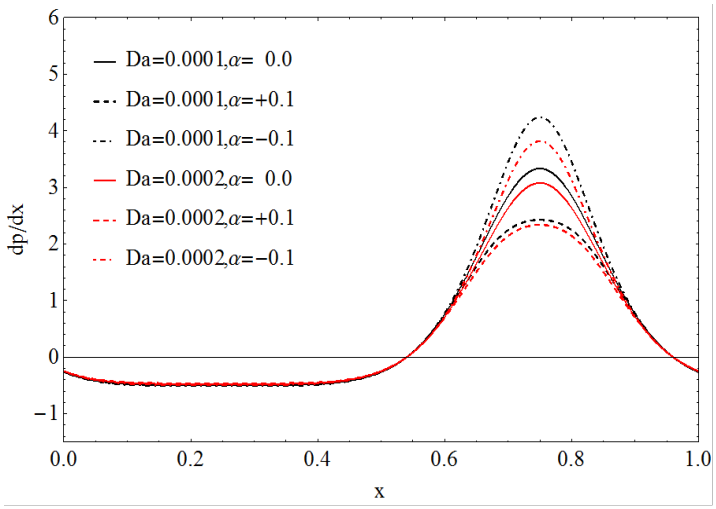

Figure 8. Pressure gradient for different values of Da, α. at $\phi = 0.3,\ Q = 0.1, \eta = 0.2$

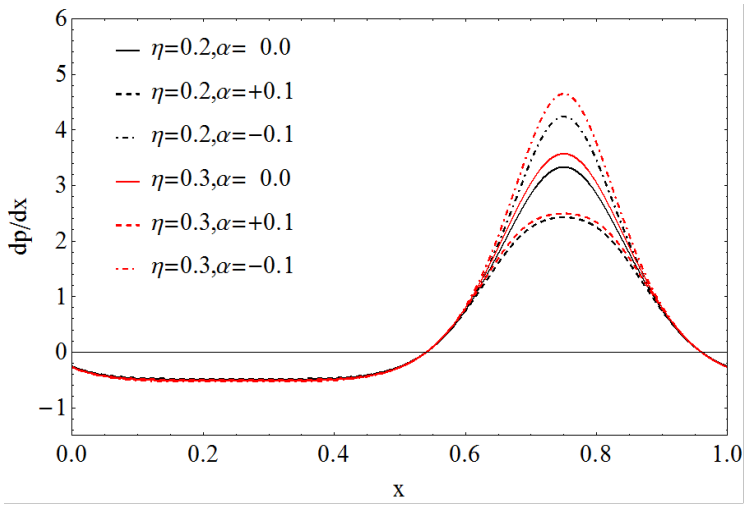

Figure 9. Pressure gradient for different values of η, α. at $\phi = 0.3, Q = 0.1, Da = 0.0001$

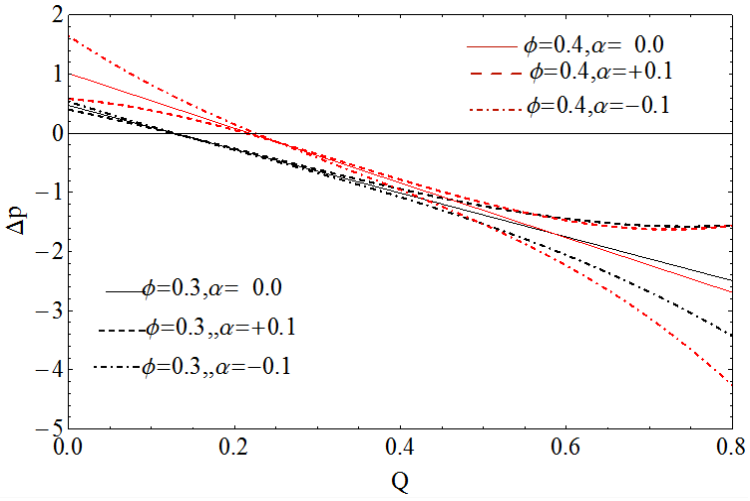

Figure 10. Pressure rise vs. flow rate for different values of ϕ, α at $Da = 0.0001, \eta = 0.5$

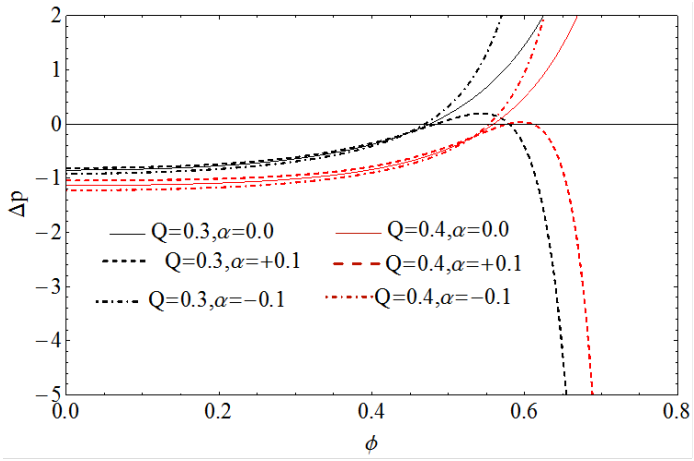

Figure 11. Pressure rise vs. amplitude ratio for different values of Q, α at $Da = 0.0001, \eta = 0.5$

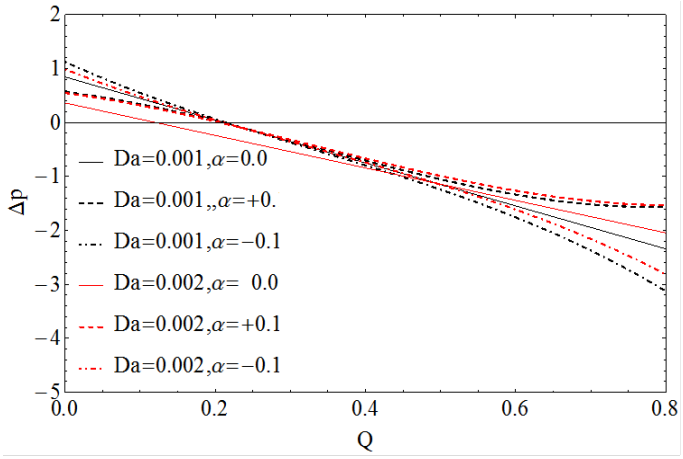

Figure 12. Pressure rise vs. flow rate for different values of Da, α at $\phi = 0.4\,, \eta = 0.5$

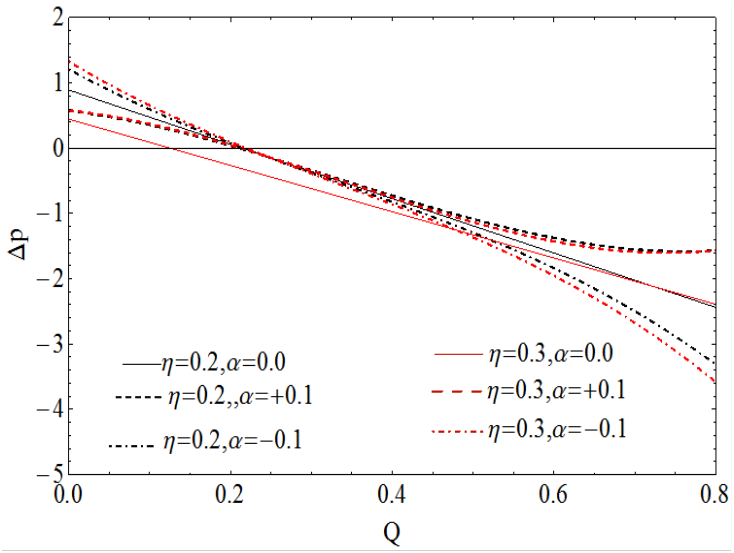

Figure 13. Pressure rise vs. flow rate for different values of η, α at $\phi = 0.4\,, Da = 0.0001$

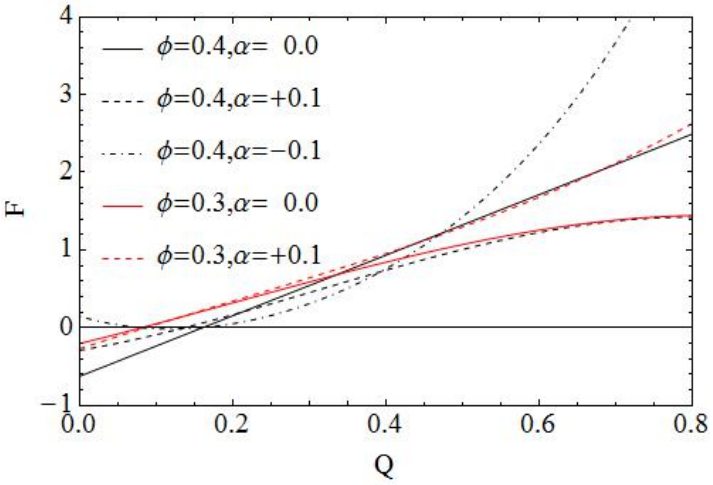

Figure 14. Frictional force vs. flow rate for different values of ϕ, α at $Da = 0.4$, $\eta = 0.5$

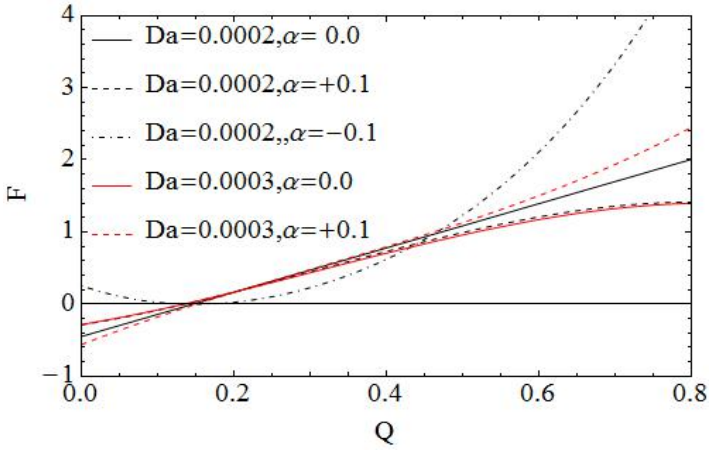

Figure 15. Frictional force vs. flow rate for different values of Da, α at $\phi = 0.4$, $Q = 0.4, \eta = 0.5$

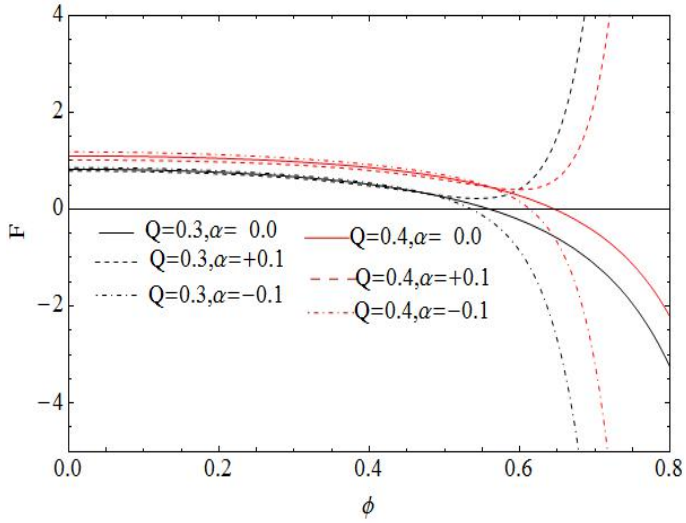

Figure 16. Frictional force vs. ampltude ratio for different values of Q, α at $\phi = 0.4$, $Da = 0.001, \eta = 0.5$

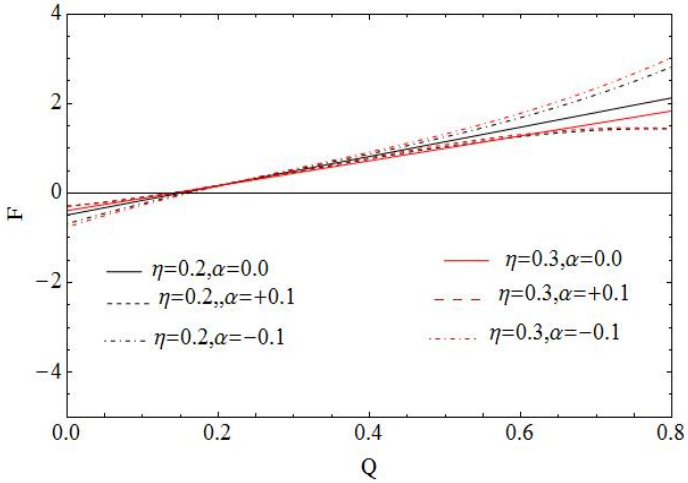

Figure 17. Frictional force vs. flow rate for different values of η, α at $\phi = 0.4$, $Da = 0.0001$

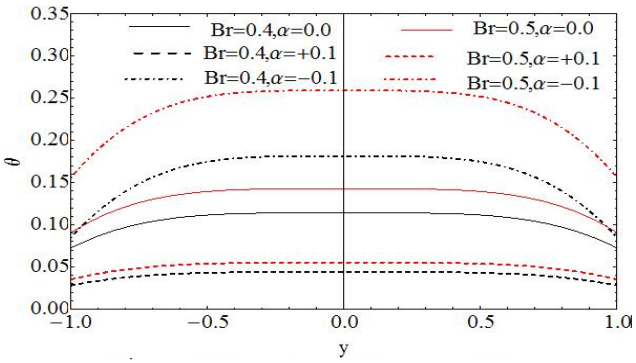

Figure 18. Effect of Br, α on temperature at $\phi = 0.3, Q = 0.8, x = 0.2, Da = 0.001, \eta = 0.2$

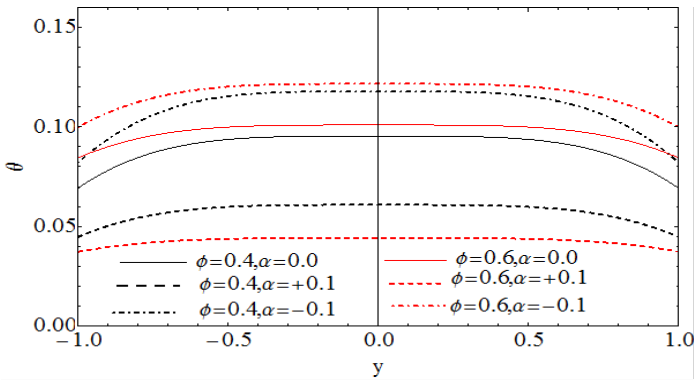

Figure 19. Effect of ϕ, α on temperature at $Da = 0.001, \eta = 0.1, Q = 0.8, x = 0.2, Br = 0.2$

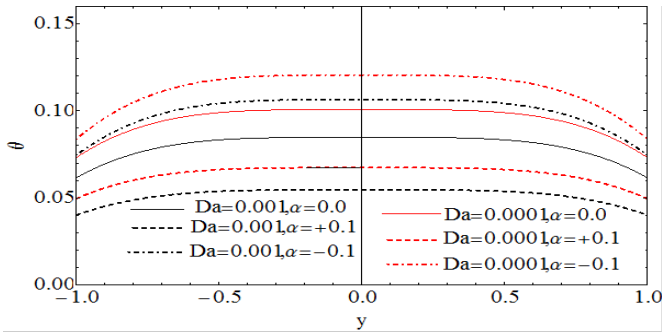

Figure 20. Effect of Da, α on temperature at $\phi = 0.4, \eta = 0.1, Q = 0.8, x = 0.2, Br = 0.2$

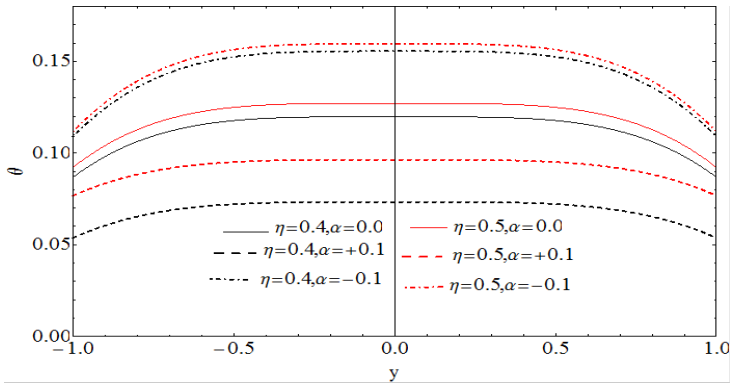

Figure 21. Effect of η, α on temperature at $\phi = 0.4, Da = 0.0001, Q = 0.8, x = 0.2, Br = 0.2$

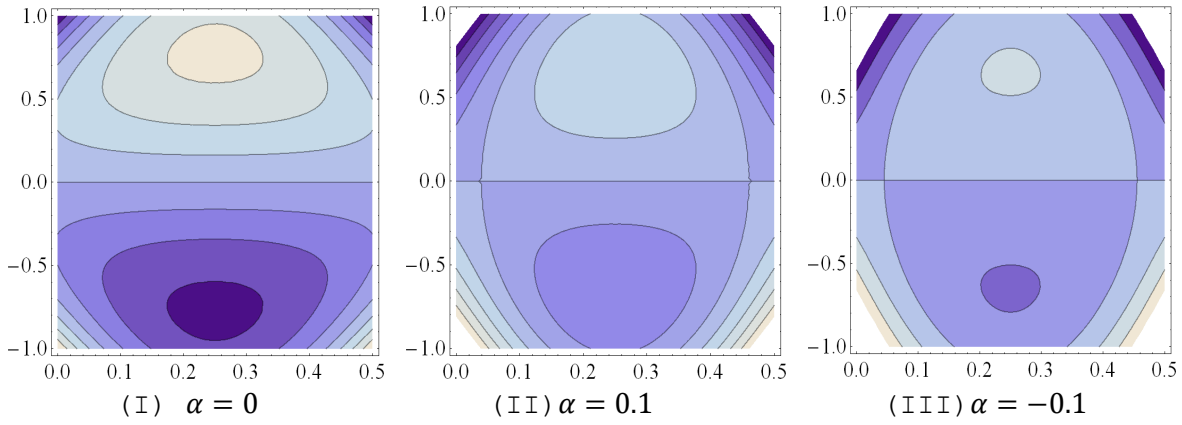

Figure 22. Stream lines when $Q = 0.8, \phi = 0.6,\ Da = 0, \eta = 1$

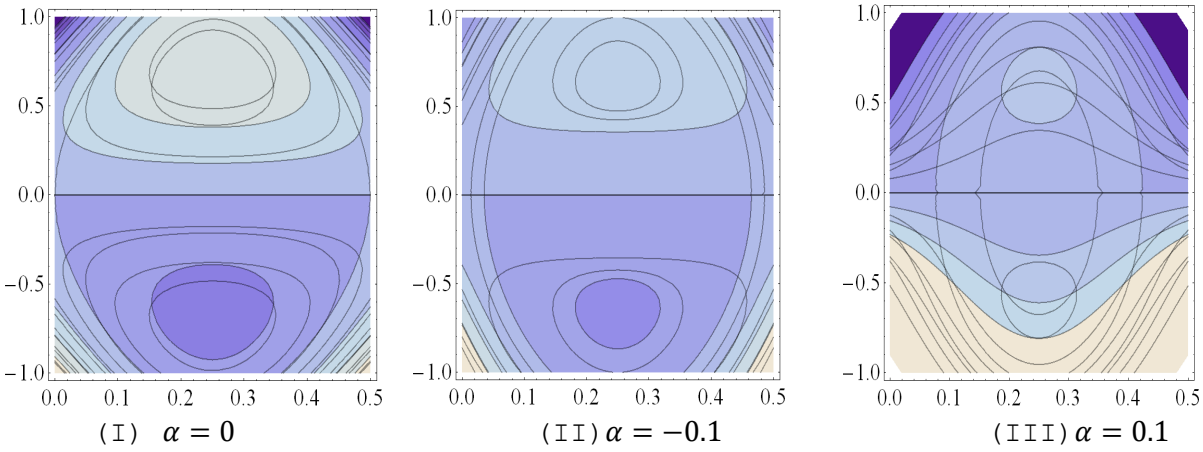

Figure 23. Stream lines when $Da = 0.0001, 0.001, 0.01$ for fixed value of $Q = 0.8, \phi = 0.6$

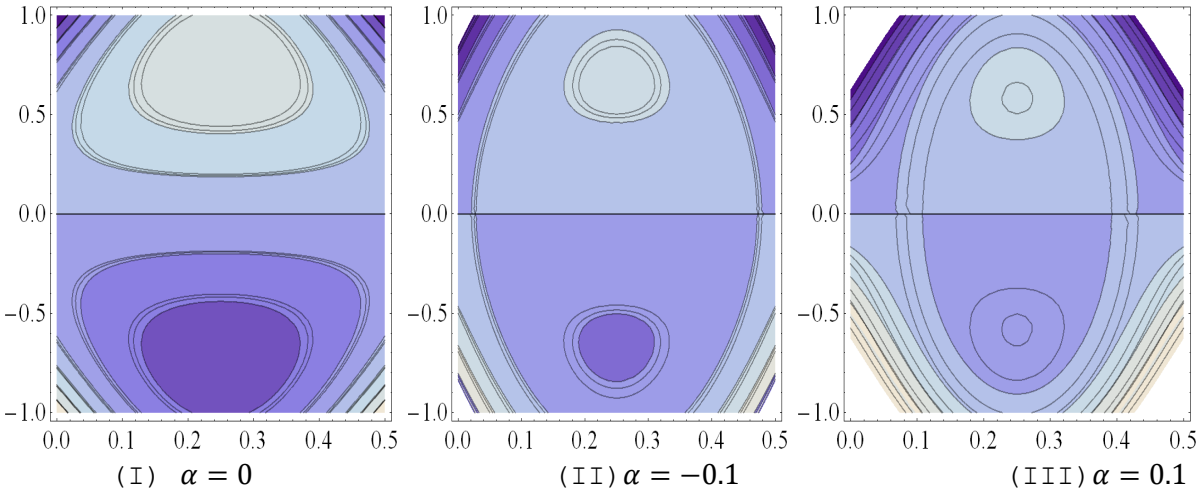

Figure 24. Stream lines when $\eta = 0.4, 0.5, 0.6$ for fixed value of $Q = 0.8, \phi = 0.6, Da = 0.001,$